UNIVERSIDADE FEDERAL DO RIO GRANDE DO SUL
ESCOLA DE ENGENHARIA - CURSO DE ENGENHARIA MECÂNICA
TRABALHO DE CONCLUSÃO DE CURSO

NUMERICAL STUDY ON THE HYDRODYNAMIC RESPONSE OF PULSATILE BLOOD FLOW IN A VEIN WITH AXISYMMETRIC STENOSIS

by

Lorenzo Ayub Salvatori

Monography presented to the Department of Mechanical Engineering of the Federal University of Rio Grande do Sul, as part of the requirements to obtain the degree of Mechanical Engineer.

Porto Alegre, February of 2024

CIP - Catalogação na Publicação

Ayub Salvatori, Lorenzo
Numerical study on the hydrodynamic response of pulsatile blood flow in a vein with axisymmetric stenosis / Lorenzo Ayub Salvatori. -- 2024.
27 f.
Orientador: Guilherme Henrique Fiorot.

Coorientador: Gustavo Pires Villela de Almeida.

Trabalho de conclusão de curso (Graduação) -- Universidade Federal do Rio Grande do Sul, Escola de Engenharia, Curso de Engenharia Mecânica, Porto Alegre, BR-RS, 2024.

1. Fluidodinâmica Computacional. 2. Modelos Reológicos. 3. Escoamento Pulsátil. 4. Vaso Sanguíneo. I. Henrique Fiorot, Guilherme, orient. II. Pires Villela de Almeida, Gustavo, coorient. III. Título.

Elaborada pelo Sistema de Geração Automática de Ficha Catalográfica da UFRGS com os dados fornecidos pelo(a) autor(a).

Lorenzo Ayub Salvatori

NUMERICAL STUDY ON THE HYDRODYNAMIC RESPONSE OF PULSATILE BLOOD FLOW IN A VEIN WITH AXISYMMETRIC STENOSIS

THIS MONOGRAPHY WAS JUDGED ADEQUATE AS PART OF THE REQUIREMENTS TO OBTAIN THE TITLE OF
MECHANICAL ENGINEER
APPROVED IN ITS FINAL FORM BY THE EXAMINING BOARD OF THE MECHANICAL ENGINEERING COURSE

Prof. Prof. Dr. Ignácio Iturrioz
Coordinator of the Mechanical Engineering Course

Concentration Area: Energy and Transport Phenomena

Advisor: Prof. Dr. Guilherme Henrique Fiorot
Co-Advisor: Dr. Gustavo Pires Villela de Almeida

Evaluation Committee:

Prof. Dr. Guilherme Henrique Fiorot (President)

Prof. Dr. Cirilo Seppi Bresolin

Prof. Dr. Fernando Marcelo Pereira

Prof. Dr. Diogo Elias Da Vinha Andrade

ACKNOWLEDGMENTS

Below, I express my gratitude to the people who were essential not only for the development of this work but also for my entire academic journey.

I would like to thank my parents, Carlos and Maria José, for their invaluable assistance in my education and development, not to mention all the support and affection they have always provided.

I thank my dear friends Francisco, Luis Henrique, Felipe K., Cristiano, Matheus C., Isabela, and Gustavo for always being next to me in my good and bad times. Their constant support and encouragement have always motivated me to be a better person.

Special thanks to my advisor Professor Fiorot, for his guidance, trust, and genuine concern for my professional and personal growth. Thank you for being an example for me.

I extend my sincere thanks to my friends from the Mechanical Engineering course, Matheus L. and Guilherme, for all their companionship and for growing alongside me throughout this journey.

I would also like to express my gratitude to my colleagues at Engys: Andre C., André D., Dário, Emanuel, Felipe S., Julio, Nicoly, Pedro, Cristian, and Lorenzo K., for being extremely warm people who genuinely care about my academic and individual development. To my co-supervisor and internship supervisor Gustavo, for his substantial contribution to my growth as a person and professional as well as being a role model for me. I am grateful to my boss, Lisandro, whose trust and motivation made this work possible.

EPIGRAPH

"You keep on learning and learning, and pretty soon you learn something no one has learned before."

Richard Feynman

UNIVERSIDADE FEDERAL DO RIO GRANDE DO SUL
ESCOLA DE ENGENHARIA - CURSO DE ENGENHARIA MECÂNICA
TRABALHO DE CONCLUSÃO DE CURSO – 2023

NUMERICAL STUDY ON THE HYDRODYNAMIC RESPONSE OF PULSATILE BLOOD FLOW IN A VEIN WITH AXISYMMETRIC STENOSIS

Salvatori, Lorenzo Ayub
lorenzoayub@gmail.com

Resumo. No contexto médico, a estenose (constrição) de um vaso sanguíneo é o estreitamento anormal de sua seção transversal, causado pelo acúmulo de placas nas paredes do vaso. Esses estreitamentos podem ocasionar diferentes problemas de saúde, dependendo da localização e severidade. Do ponto de vista fluidodinâmico, constrições em canais podem gerar zonas de recirculação, onde há maior propensão para o acúmulo de partículas suspensas no fluido. Assim, o presente trabalho avaliou, a partir de simulações em CFD, parâmetros fluidodinâmicos do escoamento pulsátil de sangue em uma veia com estenose axissimétrica. Diferentes modelos reológicos para representação do sangue foram consideradas. Inicialmente, o sangue foi modelado como um fluido newtoniano que segue o modelo de Einstein, considerando a influência da concentração de eritócitros (hematócrito) sob os parâmetros do escoamento. Subsequentemente, foram utilizados os modelos não newtonianos de Carreau e Cross. Os campos de velocidades, comprimentos de recirculação e campos de tensões cisalhantes foram analisados. Dentre as simulações em que o modelo de Einstein foi utilizado, a que considerou o valor de hematócrito mais elevado obteve as respostas mais semelhantes com as retornadas pelos modelos de Carreau e Cross. Os comprimentos de recirculação médios mais elevados foram obtidos quando utilizado o modelo de Cross.

Palavras-Chave: Estenose, Vaso Sanguíneo, Escoamento Pulsátil, Modelos Reológicos, Recirculação, CFD

Abstract. *In the medical context, the stenosis (constriction) of a blood vessel is the abnormal narrowing of its cross-section, caused by the accumulation of plaques on the vessel walls. Depending on their location and severity, these narrowings can lead to different health problems. From a fluid dynamics perspective, constrictions in channels can create recirculation zones, where there is a greater propensity for the accumulation of fluid suspended particles. Thus, the present work evaluated the fluid dynamic response of pulsatile blood flow in a vessel with axisymmetric stenosis, using CFD simulations. Different rheological models for representing blood were considered. Initially, the blood was modeled as a Newtonian fluid following the Einstein model, considering the influence of erythrocyte concentration (hematocrit) on flow parameters. Subsequently, the non-Newtonian models of Carreau and Cross were used. Velocity fields, flow recirculation lengths and shear stress fields were analyzed. The simulation results obtained using the Einstein model showed that the model yielded similar responses to those obtained from the Carreau and Cross models when the highest hematocrit value was considered. The longest average recirculation lengths were obtained when using the Cross model.*

Keywords: Stenosis, Blood Vessel, Pulsatile Flow, Rheological Models, CFD

List of Figures

List of Tables

NOMENCLATURA

Abbreviations and acronyms

BFS Backward-Facing Step

CFD Computational Fluid Dynamics

CFL Courant-Friedrichs-Lewy

CSV Comma-Separated Values

GCI Grid Convergence Index

HPC High Performance Computing

IVC Inferior Vena Cava

MRI Magnetic Resonance Imaging

RBC Red Blood Cell

WSS Wall Shear Stress

Symbols

α	Womersley Number	
$\Delta \mathrm{WSS}_{x,cs}$	Difference of $\mathrm{WSS}_{x,cs}$ at t and $t-\kappa$, averaged in domain's length	Pa
$\Delta p_{\mathrm{probes}}$	Pressure Difference Between Probes	Pa
$\dot{\gamma}$	Shear Rate	s^{-1}
$\dot{m}_A^*$	Dimensionless Amplitude of Mass Flow Rate Pulsation	
$\dot{m}_A$	Amplitude of Mass Flow Rate Pulsation	$\mathrm{kg}\cdot\mathrm{s}^{-1}$
$\dot{m}_M$	Average Mass Flow Rate Pulsation	$\mathrm{kg}\cdot\mathrm{s}^{-1}$
κ	Pulsation Period	s
λ	Transition Constant	
μ	Dynamic Viscosity	$\mathrm{Pa}\cdot\mathrm{s}$
μ_0	Low Shear Rate Viscosity	$\mathrm{Pa}\cdot\mathrm{s}$
μ_∞	High Shear Rate Viscosity	$\mathrm{Pa}\cdot\mathrm{s}$
μ_P	Blood's Plasma Viscosity	$\mathrm{Pa}\cdot\mathrm{s}$
ν	Kinematic Viscosity	$\mathrm{m}^2\cdot\mathrm{s}^{-1}$
ω	Angular Frequency	$\mathrm{rad}\cdot\mathrm{s}^{-1}$
$\overline{\mathrm{WSS}}_{x,cs}$	Average of $\mathrm{WSS}_{x,cs}$ between t and $t-\kappa$	Pa

Ψ	Hematocrit Value	
ρ	Specific Mass	$\mathrm{kg \cdot m^{-3}}$
τ	Shear Stress	Pa
τ_0	Yield Stress	Pa
θ	Phase Lag	
C	Courant Number	
C_{max}	Maximum Courant Number	
D	Tube/Vessel Diameter	m
F	Dimensionless Pulsation Frequency	
f	Pulsation Frequency	Hz
f_R	Richardson Extrapolation	
k	Fluid Consistency Index	
L_d	Entrance Lenght	m
m	Power-Law Index	
n	Flow Index	
R	Tube/Vessel Radius	m
Re	Reynolds Number	
$Re_{eff,p}$	Peak Effective Reynolds Number	
Re_{eff}	Effective Reynolds Number	
Re_M	Average Reynolds Number	
Re_p	Peak Reynolds Number	
T	Corporal Temperature	K
u	Velocity component in x direction	$\mathrm{m \cdot s^{-1}}$
u_A^*	Dimensionless Amplitude of Velocity Pulsation	
U_a	Amplitude of Velocity Inlet Function	$\mathrm{m \cdot s^{-1}}$
u_A	Amplitude of Velocity Pulsation	$\mathrm{m \cdot s^{-1}}$
U_{max}	Flow Maximum Velocity	$\mathrm{cm \cdot s^{-1}}$
U_m	Average of Velocity Inlet Function	$\mathrm{m \cdot s^{-1}}$
u_M	Mean Velocity (Averaged In Cycle And Cross-Section)	$\mathrm{m \cdot s^{-1}}$
$\mathrm{WSS}_{x,cs}$	Wall Shear Stress in x-direction averaged over the cross-section	Pa
WSS_x	Wall Shear Stress in x-direction	Pa

SUMMARY

1. INTRODUCTION

1.1. Blood

Blood is a fluid composed of a concentrated suspension of RBCs (red blood cells, also known as erythrocytes), white cells (leukocytes), and numerous oval-shaped platelets within the plasma - an aqueous solution of various proteins. Typical values for erythrocytes, leukocytes, and platelets diameters are 6-8 μm, 7-22 μm, and 2-4 μm, respectively. Since the erythrocyte volume fraction substantially exceeds the fraction of any other component, it is common to consider RBCs as the only suspension within plasma. (BERIS et al., 2021)

According to E. Fatahian, Kordani, and H. Fatahian (2018), blood viscosity is mainly determined by four factors: plasma viscosity; RBCs aggregation and deformability; hematocrit (which is the RBC concentration), and corporal temperature. Among them, the hematocrit and the RBCs aggregation and deformability are those that contribute the most to blood's non-Newtonian characteristics of shear-thinning viscosity and yield stress.

1.2. Atherosclerosis

Atherosclerosis is a vascular pathology that has been a major cause of mortality in developed countries. The term "atherosclerosis" has a Greek origin, consisting of two parts: *atherosis* (accumulation of fat accompanied by several macrophages) and *sclerosis* (fibrosis layer comprising smooth muscle cells (SMC), leukocyte, and connective tissue). (RAFIEIAN-KOPAEI et al., 2014)

It consists of the progressive narrowing and occlusion of blood vessels caused by hyperlipidemia and lipid oxidation (RAFIEIAN-KOPAEI et al., 2014). Due to the deposition of small cholesterol/fatty particles in the vessel's tunica intima (see Figure 1), a plaque (called atheroma plaque) is formed. Restricting the flow through the vessels, it can potentially result in a heart attack if the vessel being blocked supplies blood to the heart. (WAITE; FINE, 2007)

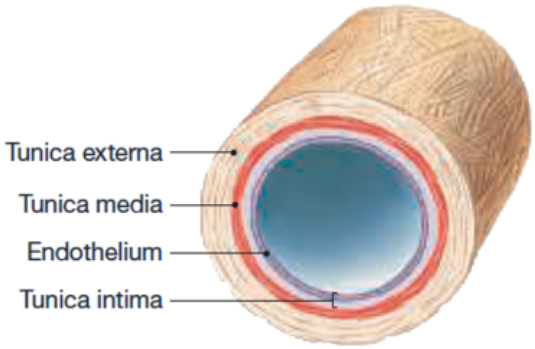

Figure 1 – Blood vessel simplified anatomy. Adapted from Almeida (2021)

Atherosclerosis can also lead to a blood clot formation, that could eventually result in a stroke. In addition, if a piece of the atheroma plaque breaks away from the vessel's wall and flows downstream, it can become lodged in smaller vessels, also potentially resulting in a stroke. (WAITE; FINE, 2007)

From a medical perspective, the abnormal narrowing of the cross-sectional area of a blood vessel or valve is called stenosis. That way, atherosclerosis can be thought of as the vascular pathology in which the blood vessel stenosis is caused by the atheroma plaque.

In a fluid dynamics context, constrictions in channels (such as stenosis in blood vessels) can create recirculation zones, where there is a greater propensity for the accumulation of fluid suspended particles. From an atherosclerosis perspective, recirculation zones next to the stenosis could promote greater fatty particles/cholesterol deposition, feeding back the atherosclerosis process.

1.3. Objectives

The present work will evaluate, from CFD simulations, fluid dynamic parameters of pulsatile blood flow in a vessel with an axisymmetric stenosis, considering different rheological models to represent blood. Initially, the blood will be modeled as a Newtonian fluid that follows Einstein's model, considering the influence of hematocrit on fluid parameters. Next, the non-Newtonian models of Carreau and Cross will be used. That way, it will be possible to analyze the velocity fields in the domain, flow recirculation lengths, and shear stresses for each rheological model.

2. THEORETICAL FOUNDATION

2.1. Non-Newtonian models for blood

At low shear rates, blood acts as a non-Newtonian fluid with shear thinning behaviour (WAITE; FINE, 2007). Nevertheless, for high shear rates (above 100 s^{-1}), its behavior is close to that of a Newtonian fluid (WAITE; FINE, 2007). In this section, the rheological models for representing blood used in the work will be presented in more detail.

2.1.1. Einstein model

The Einstein's hematocrit-dependent model for blood considers erythrocytes as blood's only suspension particles within the plasma, assuming its format as spheres. It relates the blood viscosity with the blood's plasma viscosity μ_P, the blood's hematocrit value Ψ, and the corporal temperature T, as represented by Equation 2.1 (WAITE; FINE, 2007).

$$\begin{gathered} \mu(\psi) = \mu_P \left(\frac{1}{1-\beta\psi} \right) \text{ such that} \\ \beta = 0,076 \exp\left[2,49\psi + \frac{1107}{T} exp\left(-1,69\psi\right) \right] \end{gathered} \tag{2.1}$$

The blood's hematocrit value Ψ varies from 0% (representing no erythrocytes) to 100% (representing a blood 100% erythrocyte). This value varies from 42 to 45% in healthy males, according to Waite and Fine (2007). A person is considered anemic if their hematocrit falls below 25%.

However, the change in hematocrit value implies a change in the whole blood's specific mass, as investigated by Burstain et al. (1994). This relation can be approximated as shown in Equation 2.2 and goes in agreement with the literature

data for normal blood density with physiological values of hematocrit ranging from 38 to 50%.

$$\rho = 1026 + 57,8\Psi \tag{2.2}$$

2.1.2. Carreau model

The Carreau model for representing non-Newtonian fluids is defined according to the following equation:

$$\mu(\dot{\gamma}) = \mu_\infty + (\mu_0 - \mu_\infty)\left[1 + (\lambda\dot{\gamma})^2\right]^{\frac{n-1}{2}} \tag{2.3}$$

where μ_∞ is the high shear rate viscosity; μ_0, the viscosity at low shear rates; λ is a time constant that represents the transition range in which the viscosity ceases to be constant and starts to decrease. At low shear rates, a Carreau fluid behaves similarly to a Newtonian fluid.

The article of Cho and Kensey (1991) shows a good fit between the blood's viscosity experimental data from different authors and the Carreau model equation. Cho and Kensey (1991) also provide the coefficients for the present model:

$$\begin{cases} \lambda = 3,313\ s \\ n = 0,3568 \\ \mu_0 = 0,056\ Pa \cdot s \\ \mu_\infty = 0,00345\ Pa \cdot s \end{cases}$$

2.1.3. Cross model

The Cross model is often applied in simulations for modeling the blood flow in large arteries since it generates a shorter range of viscosities in low and high shear rate regions (KARIMI et al., 2014). It follows Equation 2.4.

$$\mu(\dot{\gamma}) = \mu_\infty + \frac{\mu_0 - \mu_\infty}{1 + (\lambda\dot{\gamma})^m} \tag{2.4}$$

where m is the power-law index. In the context of blood modeling, Cho and Kensey (1991) provides the coefficients for the present model:

$$\begin{cases} \lambda = 1,007\ s \\ m = 1,028 \\ \mu_0 = 0,056\ Pa \cdot s \\ \mu_\infty = 0,00345\ Pa \cdot s \end{cases}$$

2.2. Channel Entrance Length

For internal flows in ducts/tubes, the entrance length is defined as the distance measured from its inlet to the point where the flow is said to be fully developed (FOX; MCDONALD, A.; PRITCHARD, 2018). Fox, A.T. McDonald, and Pritchard (2018) present an empirical relation for estimating the entrance length on laminar flows in ducts/tubes:

$$\frac{L_d}{D} \approx 0,06Re \tag{2.5}$$

Ray, Ünsal, and Durst (2012) studied the development length in pipes with laminar sinusoidally pulsating flows. The relation obtained by the authors to estimate the maximum development length is shown in Equation 2.6.

$$\left(\frac{L_d}{D}\right)_{max} = \left[(0,619)^{1,6} + (0,0567Re_M)^{1,6}\right]^{1/1,6} \left[1 + C_L + \frac{\dot{m}_A^* - C_L}{1 + (\frac{F}{3,25})^3}\right] \quad (2.6)$$

where D represents the pipe diameter, Re_M represents the flow's average Reynolds number (Equation 2.7) and $\dot{m}_A^*$ is the dimensionless amplitude of the mass flow rate pulsation, defined in Equation 2.9. In their work, it is shown that $\dot{m}_A^*$ equals $\dot{u}_A^*$ - the dimensionless amplitude of velocity pulsation (Equation 2.8).

$$Re_M = \frac{\rho u_M D}{\mu} \quad (2.7)$$

$$\dot{u}_A^* = \frac{u_A}{u_M} \quad (2.8)$$

$$\dot{m}_A^* = \frac{\dot{m}_A}{\dot{m}_M} \quad (2.9)$$

In addition, C_L is a function of $\dot{m}_A^*$ (Equation 2.11) and F is the dimensionless pulsation frequency, defined from pulsation frequency f (Equation 2.10).

$$F = \frac{R^2 f}{\nu} \quad (2.10)$$

$$C_L = 0,1671(\dot{m}_A^*)^{1,1881} \quad (2.11)$$

2.3. Womersley Number

The Womersley number α is a dimensionless parameter that indicates the distance to the laminar velocity profile in a long vessel coincides with the Poiseuille flow profile when the fluid is subjected to a sinusoidal pressure gradient (CARO et al., 2011). It is defined as:

$$\alpha = R\left(\frac{\omega\rho}{\mu}\right)^{1/2} = R\left(\frac{\omega}{\nu}\right)^{1/2} \quad (2.12)$$

where R is an appropriate characteristic length (generally the vessel radius) and ω is the oscillatory frequency of the flow in rad/s.

The Womersley number may also be considered an "unsteady Reynolds number" for the flow since it indicates the proportion of inertial and viscous forces in motion determination within the time scale of one period of oscillation (CARO et al., 2011).

When α is small (less than unity), the flow is 'quasi-steady' and its velocity magnitude is determined by the instantaneous pressure gradient, with the profile being parabolic at all times. In that scenario, viscous forces are dominant, and inertial forces could be neglected (CARO et al., 2011).

For large values of α, the fluid volume set in motion by the wave passage is big when compared to the volume of fluid that is delayed due to the wall's no-slip

condition (the boundary layer is thin). Thus, viscous forces could be neglected and inertial forces are dominant (CARO et al., 2011).

Caro et al. (2011) also pointed out that α^2 is the ratio between the time necessary for the viscous forces to diffuse across the whole tube width $(d^2/4\nu)$ and a characteristic time of the oscillation period $(1/\omega)$.

$$\frac{\text{transient inertial force}}{\text{viscous force}} = \frac{\rho\omega U}{\mu U L^{-2}} = \frac{\rho\omega L^2}{\mu} = \frac{\omega L^2}{\nu} = \alpha^2$$

3. METHODOLOGY

In this chapter, it will be presented the work methodology in detail.

3.1. Geometry

For the present work, it will be considered a constant diameter of 1 cm for both expiratory and inspiratory phases, i.e., it will be considered rigid vessel walls with a diameter of 1 cm. The constriction severity (d/D) will be considered as being 0,5 (see Figure 2).

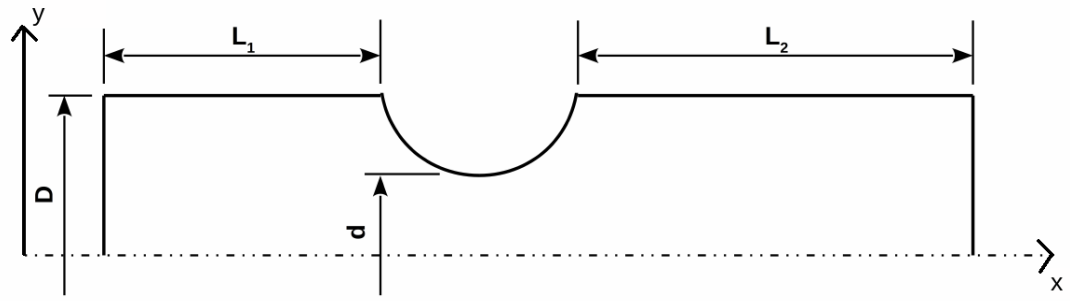

Figure 2 – Constricted channel geometry. Adapted from Almeida (2021)

The length of L_1 will be estimated given that the flow can be considered fully developed (considering the peak Reynold number) before reaching the constriction. From Equation 2.6, it is obtained an entrance length of 22,30 cm. However, by using Equation 2.5, the entrance length estimative 39,89 cm. As the entrance length calculated by Equation 2.5 is greater than the one from Ray, Ünsal, and Durst (2012) relation, the first one is going to be used as a reference. It will be considered $L_1 = 42,5$ cm. That way, the constriction center is located at $x = 45$ cm.

The constriction to outlet length L_2 has to be extensive enough so that all recirculation zones and flow perturbations are observed. From a study of the effects of blood's non-Newtonian behavior on the laminar-turbulent transition over a BFS geometry, Kelly et al. (2020) obtained a maximum primary recirculation zone in $Re \cong 1200$ where $x_1/S \cong 13,1$, representing S the step size and x_1 the recirculation length. Although the study was performed considering a turbulent non-pulsatile flow, this relation for the maximum primary recirculation zone will be used as a reference for this work.

Assuming S as being $d/2$ in the constricted vessel geometry, the maximum primary recirculation zone x_1 equals 3,275 cm. Considering that the flow could have other recirculation zones, and to ensure that all flow perturbations will be observed, it will be considered $L_2 = L_1$.

3.2. Rheology models

3.2.1. Einstein Model

As mentioned in the Theoretical Foundation, Einstein's model is a function of the hematocrit value Ψ, corporal temperature T, and plasma viscosity μ_P. According to Késmárky et al. (2008), plasma viscosity value ranges from 1,1 to 1,3 $mPa \cdot s$ at 37ºC, regardless of age and gender. It will be considered μ_P as 1,2 $mPa \cdot s$ and T as 37ºC (310 K).

According to Equation 2.2, each value of hematocrit that will be used while using Einstein's model will have a corresponding value of ρ. For this work, it will be used Ψ values of 35%, 40%, 45%, and 50%. Table 1 shows the values of specific mass and viscosity for all chosen Ψ.

Table 1 – Values used in Einstein's model for ρ, β and μ as functions of Ψ

$\Psi(\%)$	$\rho(kg/m^3)$	β	$\mu(Pa \cdot s)$
35	1046,23	1,311	2,217e-3
40	1049,12	1,265	2,429e-3
45	1052,01	1,236	2,706e-3
50	1054,90	1,223	3,091e-3

3.2.2. Cross and Carreau models

For Cross and Carreau models, it will be used the respective coefficients provided by Cho and Kensey (1991), presented in the Theorical Foundation.

3.3. Boundary and Initial Conditions

The geometry is divided into three boundaries: *inlet*, *walls*, and *outlet* (as shown in Figure 3). The blood pulsation was represented by a senoidal x-component velocity inlet (Eq 3.1), where U_a is the function's amplitude and U_M its mean value. The function's phase lag θ is assumed a value of zero.

For the present work, Inferior Vena Cava (IVC) data from the literature were used to define the boundary conditions. By performing an MRI on 11 subjects, Joseph, Voit, and Frahm (2020) measured a mean velocity of $7,7(\pm 3,1)$ cm/s in the infrarenal IVC. That way, it will be considered U_M as 7,7 cm/s. Furthermore, U_a will be considered equals to U_M. That way, Equation 3.1 varies from 0 to $2U_M$.

$$u(t) = U_a \sin(2\pi f t + \theta) + U_M \tag{3.1}$$

The pulsation frequency f was set to 1,2 Hz to represent a heartbeat rate of 72 bpm. That way, the pulsation period κ is shown in Equation 3.2. Table 2 summarises the boundary and initial conditions for the case setup. In that table, n represents the positive direction normal to the patch.

$$\kappa = 0,833\overline{333} \text{ s} \tag{3.2}$$

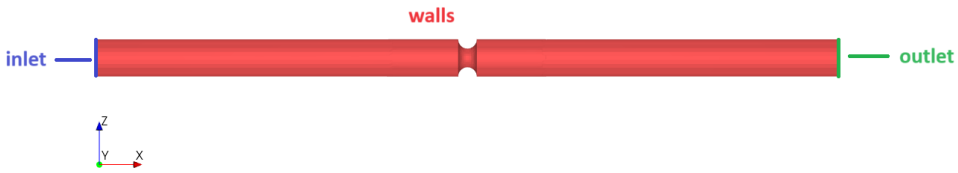

Figure 3 – Geometry boundaries (out of scale)

Table 2 – Boundary and Initial Conditions

Boundaries	Boundary Conditions		Initial Conditions ($t = 0$)	
	u	p	u	p
inlet	$u(t) = 0,077[\sin(2,4\pi t) + 1]$	$\delta p/\delta n = 0$	$u = U_M$	$\delta p/\delta n = 0$
walls	$u = 0$	$\delta p/\delta n = 0$	$u = 0$	$\delta p/\delta n = 0$
outlet	$\delta u/\delta n = 0$	$p_{gauge} = 0$	$\delta u/\delta n = 0$	$p_{gauge} = 0$

3.4. Dynamic characterization of the problem

Just like the velocity values at the input, the Reynolds number will oscillate throughout a pulsation. The average and peak Reynolds number throughout the cycle will be represented by Re_M and Re_p, respectively.

Using a blood viscosity calculated from the Einstein model for a Ψ of 40%, the Re_p was estimated, shown in Eq. 3.3. However, when dealing with oscillatory flows, the calculated Reynolds number needs to be multiplied by a correction factor which is function of the Womersley number α (see Hale, D. A. McDonald, and Womersley (1955)) to obtain an effective Reynolds number Re_{eff} (Eq. 3.4).

$$Re_p = \frac{\rho(U_a + U_m)D}{\mu} = 664 \tag{3.3}$$

$$Re_{eff} = f(\alpha) \cdot Re \tag{3.4}$$

Figure 4 shows a graph of the correction factor as a function of α. Note that, for $\alpha < 2$, the pulsation effect on the flow Reynolds is not significant. For our case, it was obtained a Womersley number of 9 (Equation 3.5). It is worth emphasizing that the literature considers that a typical value of α for a man's aorta is around 20. Even though the Vena Cava is not an aorta, the simplifications assumed to solve the problem must be also taken into account, such as:

- Constant lumen diameter during the cycle (no inspiration or expiration phases);
- Blood pulsatile flow is modeled as a sine wave and it is not a perfect representation of systole and diastole;
- Blood viscosity is assumed to be independent of the vessel diameter, desconsidering the aggregation of blood red cells.

$$\alpha = \frac{D}{2}\sqrt{\frac{\omega}{\nu}} = 9 \tag{3.5}$$

According to Fig 4, the correction factor is around 2,5, which leads to a peak Re_{eff} shown in Equation 3.6. Being an internal flow in a vessel and considering the fact that $Re_{eff,p}$ is less than 2300, it can be assumed a laminar flow in the sections without constriction.

$$Re_{eff,p} = f(\alpha) \cdot Re_p = 1162 \tag{3.6}$$

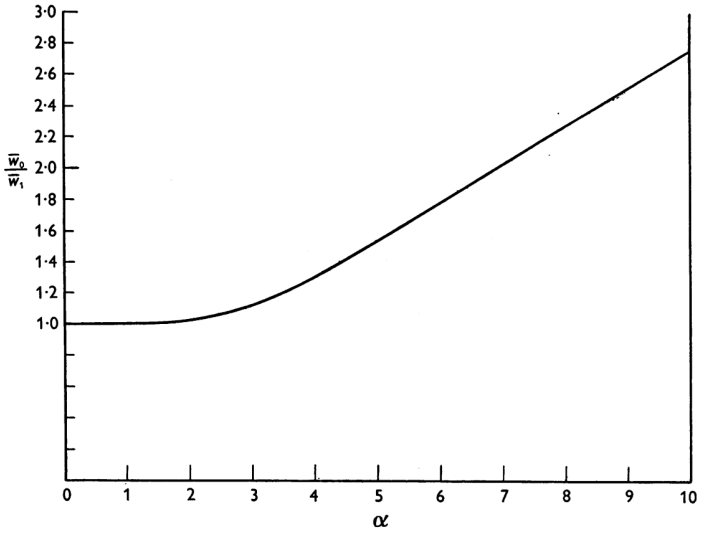

Figure 4 – Womersley number effect in the velocity ratio for oscillating flows. In that ratio, $\bar{w}_0$ represents the equivalent average velocity which will result in the same maximum viscous drag as the oscillating flow. The $\bar{w}_1$ represents the maximum forward velocity of that oscillating flow. (HALE; MCDONALD, D. A.; WOMERSLEY, 1955)

3.5. Numerical Methodology

The numerical simulations were realized in HELYX®, from Engys company. HELYX® is an open-source CFD software written in C++ programming language. Since its solvers were based on the OpenFOAM ones, it can represent several phenomena linked to fluid mechanics, thermodynamics, turbulence, rheological models, and heat transfer, among others. Even though the software does not have a student license at the present moment, the company has authorized the author to use it for this work.

The solver used for the simulations is authored and owned by Engys. For data post-processing, the open-source tool ParaView was used, in addition to HELYX®. The simulations were conducted in an HPC environment, using from 48 to 72 processors, depending on the simulation.

3.5.1. Inlet boundary

The software does not allow, at the present moment, the user to enter an analytical function as a condition of a field in the domain boundaries. However, it is

possible to enter values for a field on a boundary throughout all iterations/time steps. The values inputted by the user are then linearly interpolated over the iterations/time steps.

Thus, to represent the velocity field function at the domain input (Equation 3.1), a Python 3.9 script was written to generate a CSV file that would be read and interpreted by HELYX®. For each time step to be simulated, the script calculates the corresponding value for u and writes a line in the CSV file with this data. The code is presented in Appendix A.

3.5.2. Runtime Controls

In transient cases, it is necessary to verify the CFL (Courant-Friedrichs-Lewy) condition to guarantee the numerical stability of the solution (see Equation 3.7). Generally, an approximation is made using the Courant number where the flow velocity is used as a reference. The maximum allowed Courant number C_{max} depends on the temporal integration scheme, associated with the spatial discretization schemes. However, C_{max} is normally used as being equal to 1.

$$C = \frac{u_L \Delta t}{\Delta x} \leq C_{max} \tag{3.7}$$

By default, HELYX uses the fully implicit temporal discretization method, which is inherently stable, allowing the utilization of larger simulation time steps when compared to the implicit (semi-implicit) and explicit methods. For the simulations performed in this study, it was used a time step of $0,001$ second.

The simulation's end time was set in 16,666 seconds, which corresponds to the time of 20 wave periods (Eq. 3.1). The results were written in the simulations folder every 0,831 seconds (approximately one-third of the period).

3.6. Mesh Convergence

For the quantification of numerical uncertainty related to the mesh refinement, it was used the Grid Convergence Index (GCI), proposed by P. J. Roache (see Roache (1997)). This methodology is based on the comparison of the result of flow variables, obtained from grids with different spacing, and the realization of generalized Richardson extrapolations.

It was compared three flow variables of the problem: maximum velocity magnitude, recirculation length, and the pressure difference between two probes located at ± 5 cm of the constriction center. An application integrating Python and Bash (programming languages) was made by the author to perform this grid convergence analysis, given a set of base mesh sizes and compared parameters.

The Tables 3 and 4 show the simulation data for each mesh compared and the grid convergence indexes, respectively. In the first table, M1 represents the most refined mesh, while M3 represents the most coarse and M2 the intermediate one. For the second table, $f_{R\text{-ij}}$ represents the Richardson extrapolation value obtained from comparing M_j and M_i meshes. The same logic applies to $\mathrm{GCI}_{\mathrm{ij}}$ indexes.

4. RESULTS

In this section, the results obtained from the simulations will be presented.

Table 3 – Grid convergence analysis data for $d/D = 0,5$ geometry

	Meshes		
Variables	**M1**	**M2**	**M3**
Number of Cells	2.834.786	574.808	163.832
U_{max} (cm/s)	36,551	37,360	39,406
Δp_{probes} (Pa)	-47,232	-50,301	-62,448
Recirculation Lenght (mm)	57,270	59,960	71,030

Table 4 – GCI indexes and fields Richardson's extrapolations values for $d/D = 0,5$ geometry

Variables	U_{max}	Δp_{probes}	Recirculation Lenght
$f_{R\text{-}32}$	$36,2660922\ cm/s$	$-46,676840\ Pa$	$56,8093477\ mm$
$f_{R\text{-}21}$	$36,2660924\ cm/s$	$-46,676842\ Pa$	$56,8093479\ mm$
GCI_{32} $(\%)$	3,66	9,00	6,57
GCI_{21} $(\%)$	0,97	1,47	1,00

4.1. Wall Shear Stresses in x direction

From the wall shear stress data in *walls* patch, it was possible to extract the cross-section perimeter averaged WSS in x direction, represented by $\text{WSS}_{x,cs}$. Figures presenting the $\text{WSS}_{x,cs}$ distribution around the constriction (from $x = 0,42$ m to $x = 0,56$ m) for each of the rheological models at pre-determined simulation times can be found in Appendix B. However, Figure 5 shows $\text{WSS}_{x,cs}$ at $t/\kappa = 19,94$ from $x = 0,425$ m to $x = 0,475$ m, i.e., the constriction length.

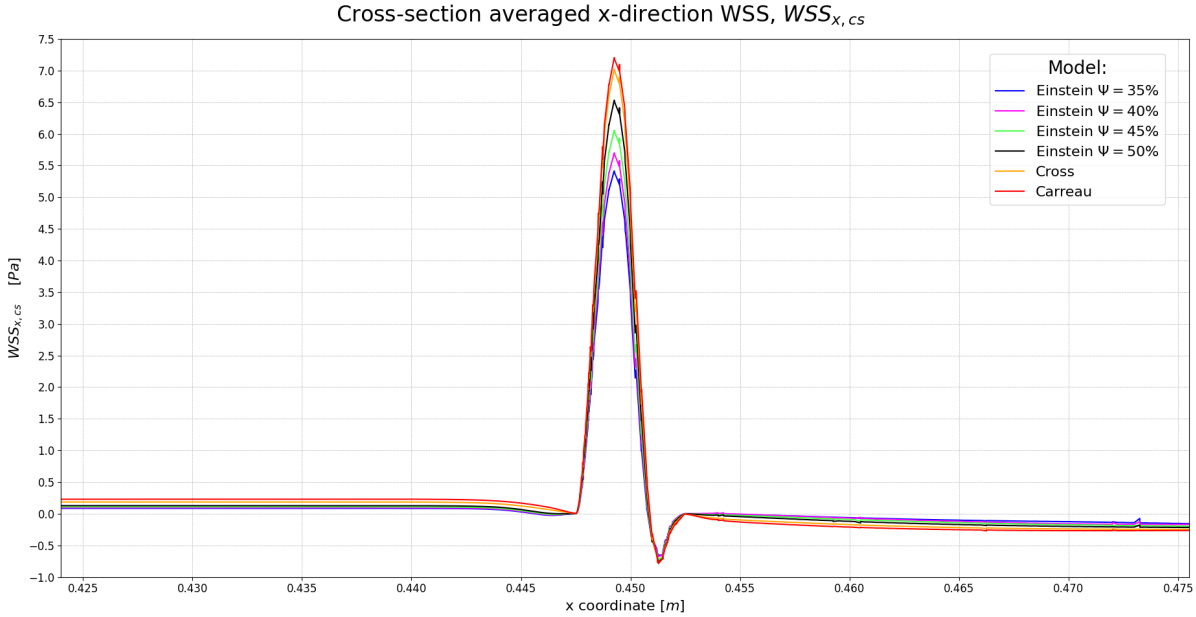

Figure 5 – $\text{WSS}_{x,cs}$ in the constriction length at $t/\kappa = 19,94$

To analyze the convergence of $\text{WSS}_{x,cs}$ distributions throughout the pulsations, the $\Delta\text{WSS}_{x,cs}$ variable was introduced (Equation 4.1). It represents the absolute

difference between the $\mathrm{WSS}_{x,cs}$ distribution of a given time and the distribution of the previous period, averaged across the domain's length.

$$\Delta\mathrm{WSS}_{x,cs}(t) = \frac{1}{0,9\ \mathrm{m}} \sum_{x_i=0\ \mathrm{m}}^{0,9\ \mathrm{m}} \mathrm{abs}\left(\mathrm{WSS}_{x,cs}(x_i)|_t - \mathrm{WSS}_{x,cs}(x_i)|_{t-\kappa}\right) \tag{4.1}$$

Figure 6 shows the variation of $\Delta\mathrm{WSS}_{x,cs}$ through simulation time. It is seen that, even after 20 pulses, the shear stress distributions for Einstein's models considering Ψ from 30 to 45% still fluctuate. However, for the Cross and Carreau models, the distributions throughout the pulsation periods appear to vary in a more regular way. In addition, the Einstein model considering Ψ as 50% behaviors similar to the non-Newtonian models.

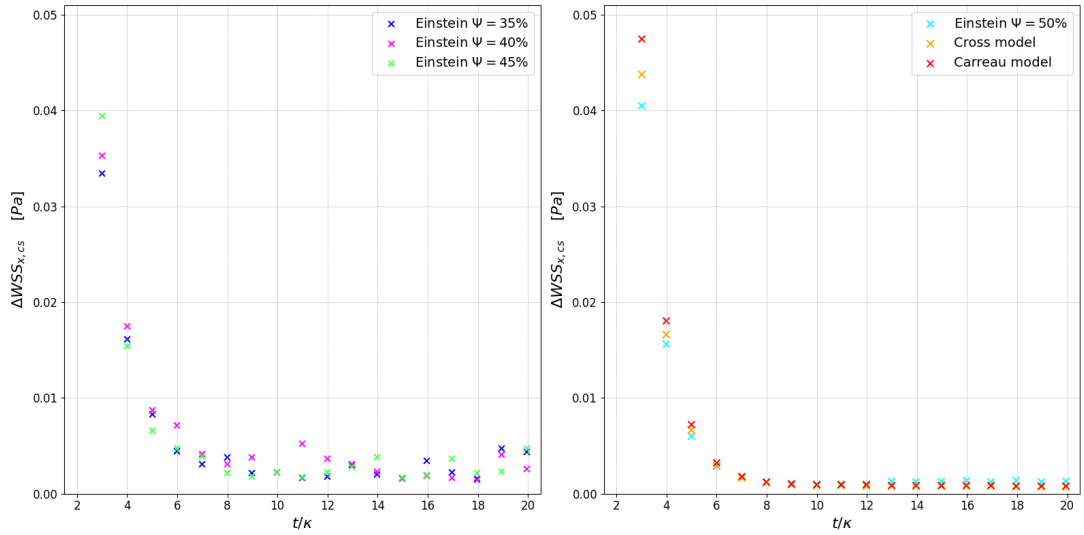

Figure 6 – $\Delta\mathrm{WSS}_{x,cs}$ throughout pulsations

It should be highlighted that there are at least two additional sources of numerical error in the above data. The first of these is associated with the precision of the time step. Even though the simulation time step is relatively small, the period is a periodic decimal. This way, the times recorded by the simulation cannot coincide with the period (which is why, for example, t/κ is shown equal to 1,99 and not 2,00). The second additional source of error occurs in the use of such shear stress data: the data was extracted from the nodes of the cell volume, and not from its center.

4.2. Velocities in x direction

To evaluate the velocity field downstream of the constriction, three surfaces were created (Figure 7) in the simulations at 2 cm (surface 01), 4 cm (surface 02), and 6 cm (surface 03) from the constriction. Figure 8 shows the velocity distributions in the x direction on the surfaces, for each of the rheological models, in $t = 16,066\ s$. The highest and lowest speeds were observed on surface 01, for the Einstein model with $\Psi = 40\%$, with values of 0,6787 m/s and -0,1451 m/s, respectively.

Note that the u distributions were very similar between the Einstein with $\Psi = 50\%$, Cross, and Carreau models on all surfaces. Furthermore, when analyzing

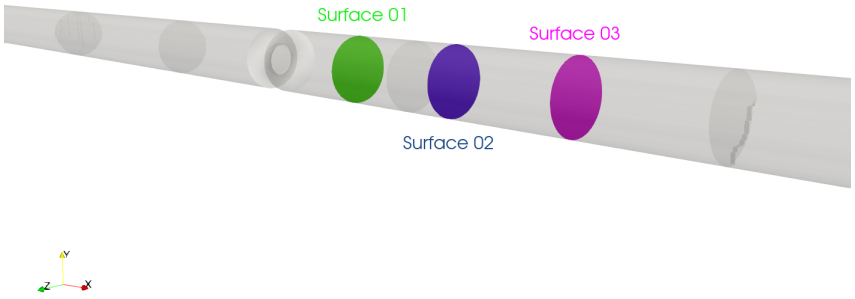

Figure 7 – Surfaces where the velocity field was analyzed

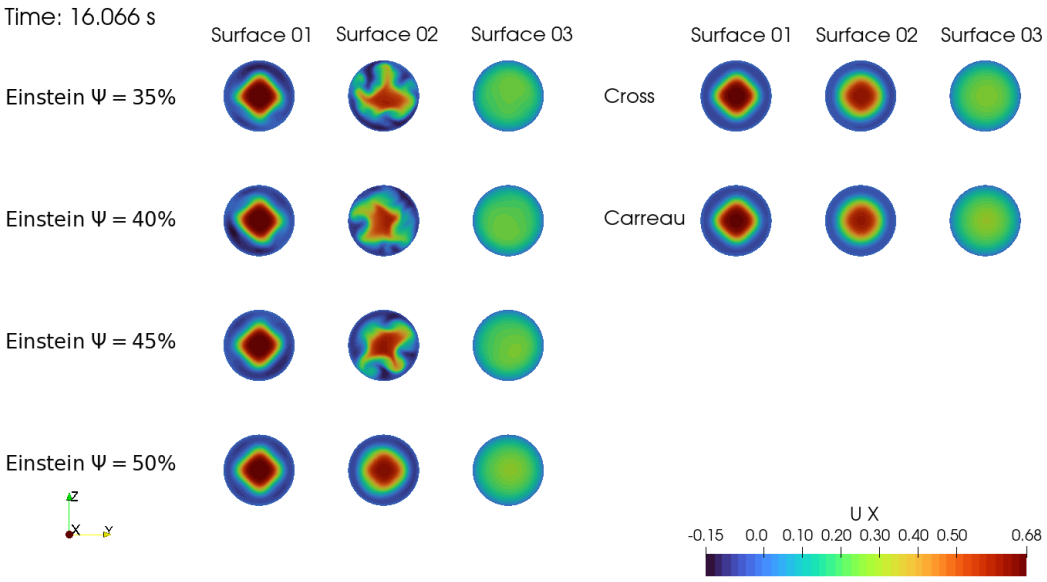

Figure 8 – Velocity in x-direction distributions in defined surfaces, for each rheological model at $t = 16,066\ s$

surface 02 for the simulations in which Einstein's models were used, it is evident that the increase in hematocrit made the flow's viscous effects more notable.

4.3. Cycle-Averaged Maximum Recirculation Lenghts

Using the function object *fieldAverage* in HELYX, it was possible to obtain a field of pulsation-averaged values of $\mathrm{WSS}_{x,cs}$, named $\overline{\mathrm{WSS}}_{x,cs}$. This new field, which represents the shear stress in x direction averaged in the cross-section and in a pulsation period, is defined in Equation 4.2 and illustrated in Figure 9.

$$\overline{\mathrm{WSS}}_{x,cs} = \frac{1}{\kappa}\int_{t-\kappa}^{t} \mathrm{WSS}_{x,cs}\, dt \tag{4.2}$$

From this field, it was possible to obtain the maximum recirculation lengths

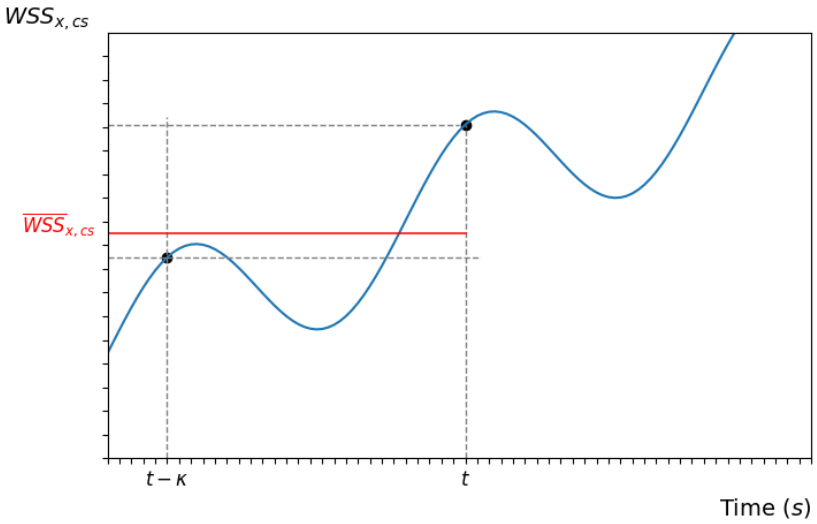

Figure 9 – Graphical example of pulsation-averaged $\mathrm{WSS}_{x,cs}$

averaged in $[t-\kappa, t]$. The recirculation length in the x direction corresponds to the extension of the domain in which the WSS_x is negative. Figure 10 shows those cycle-averaged maximum recirculation lengths for each of the rheological models.

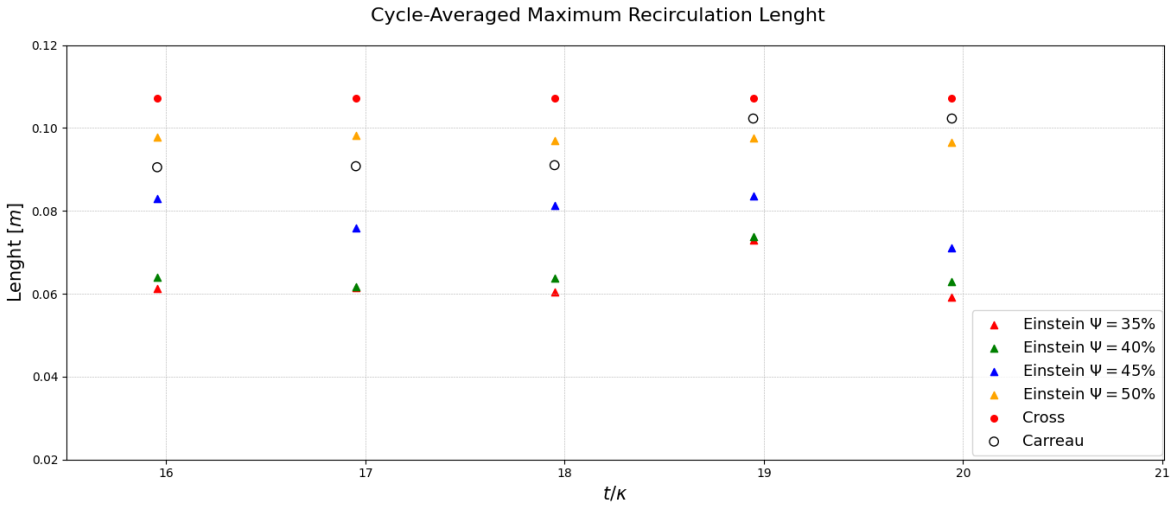

Figure 10 – Cycle-averaged maximum recirculation lengths for each one of the rheological models

From Figure 10, it can be seen that the Einstein model with Ψ of 50% has the most similar values for recirculation length to the non-Newtonian models, among all variations of Einstein models simulated. Furthermore, the recirculation lengths increased when raising Ψ values.

5. CONCLUSION

By conducting a numerical study on the fluid dynamic response of the pulsatile flow in a vein with axisymmetric stenosis, the velocity, and shear stress fields were analyzed as well as the flow recirculation lengths. Blood, often modeled as both Newtonian and non-Newtonian (depending on the specific physical context) was assessed using three distinct rheological models: Einstein, Cross, and Carreau. For the Einstein model - dependent on the hematocrit value Ψ - it was used Ψ values 35%, 40%, 45%, and 50%.

In terms of shear stress distributions, the non-Newtonian models exhibited similar profiles, displaying consistent variations throughout the pulsation periods, akin to the Einstein model with $\Psi = 50\%$. In contrast, for Einstein models with Ψ set at 35%, 40%, and 45%, the variations in shear stress distribution fluctuated over the periods.

Being a three-dimensional flow, particularly in the region immediately downstream of the stenosis, we assessed the distribution of u values on pre-defined surfaces. On the surface nearest to the constriction (Surface 01), the u distribution exhibited similarities across all rheological models. The highest and lowest u values were observed on this surface, for the Einstein model with $\Psi = 40\%$. Flow's viscous effects became more notable on surface 02 when Ψ increased. Once more, Einstein's model with $\Psi = 50\%$ produced the results more similar to those of the non-Newtonian models, among all values of Ψ. Finally, the distributions on Surface 03 showed no significant differences between the various rheological models.

Using the values of the shear stress fields averaged over a pulsation and the cross-section perimeter, it was able to present the cycle-averaged maximum recirculation lengths over x. The Cross model yielded the highest recirculation values, while Einstein's with $\Psi = 35\%$ exhibited the smallest. Among the simulated Einstein's models, the increase of Ψ yielded the higher recirculation length values and once again the simulation with Ψ of 50% obtained a response more similar to the models of Carreau and Cross.

Upon analyzing the obtained results, a substantial disparity in the hydrodynamic response was evident, as anticipated, when manipulating the hematocrit value. The fact that Einstein's model considering the greater value of Ψ ($\Psi = 50\%$) demonstrated the closest resemblance to non-Newtonian models was expected since the hematocrit is one of the main contributors to some non-Newtonian characteristics, as mentioned in Section 1.1.

Among the non-Newtonian models, a small (but significant) difference was noted in the shear stress distributions and recirculation lengths. Although such differences are expected, it is crucial to consider the potential influence of multiple sources of numerical error, as well as the spatial and temporal dependency of the flow.

5.1. Suggestions for future works

For future investigations, it is recommended further exploration studies of this simulated scenario. Regarding blood rheology, additional rheological models, such as Herschel-Bulkley, should be considered. Additionally, examining the change in the ratio between the vessel diameter and the constriction diameter (the stenosis severity) would be valuable.

Given the blood composition, modeling blood as multiphase fluid may provide more trustworthy results. Furthermore, a multiphase representation opens avenues

for analyzing the deposition rate of cholesterol particles within the vessel walls, offering a more advanced perspective for future research.

REFERENCES

ALMEIDA, G. P. V. de. **Implementation of Hematocrit-Dependent Viscosity Model for Blood Flow Predictions using CFD**. 2021. PhD thesis – Instituto Tecnológico de Aeronáutica (ITA).

BERIS, A. N. et al. **Recent advances in blood rheology: A review**. [S.l.: s.n.], 2021.

BURSTAIN, J. M. et al. Blood Volume Determination as a Function of Hematocrit and Mass in Three Preservative Solutions and Saline. **American Journal of Clinical Pathology**, v. 102, n. 6, p. 812–815, Dec. 1994. ISSN 0002-9173. DOI: 10.1093/ajcp/102.6.812.

CARO, C. G. et al. **The Mechanics of the Circulation**. 2. ed. [S.l.]: Cambridge University Press, 2011.

CHO, Y.; KENSEY, K. Effects of the non-Newtonian viscosity of blood on flows in a diseased arterial vessel. Part 1: Steady flows. **Biorheology**, v. 28, p. 241–62, Feb. 1991. DOI: 10.3233/BIR-1991-283-415.

FATAHIAN, E.; KORDANI, N.; FATAHIAN, H. A Review On Rheology of Non-Newtonian Properties Of Blood. **IIUM Engineering Journal**, v. 19, n. 1, p. 237–250, Mar. 2018. DOI: 10.31436/iiumej.v19i1.826.

FOX, R.; MCDONALD, A.; PRITCHARD, P. **Introdução à Mecânica dos Fluidos**. [S.l.]: LTC, 2018. ISBN 9788521634812.

HALE, J. F.; MCDONALD, D. A.; WOMERSLEY, J. R. Velocity profiles of oscillating arterial flow, with some calculations of viscous drag and the Reynolds number. **The Journal of Physiology**, v. 128, n. 3, p. 629–640, 1955. DOI: 10.1113/jphysiol.1955.sp005330.

JOSEPH, A. A.; VOIT, D.; FRAHM, J. Inferior vena cava revisited – Real-time flow MRI of respiratory maneuvers. **NMR in Biomedicine**, v. 33, n. 4, 2020. DOI: 10.1002/nbm.4232.

KARIMI, S. et al. Effect of rheological models on the hemodynamics within human aorta: CFD study on CT image-based geometry. **Journal of Non-Newtonian Fluid Mechanics**, v. 207, p. 42–52, 2014. ISSN 0377-0257. DOI: 10.1016/j.jnnfm.2014.03.007.

KELLY, N. S. et al. Influence of Shear-Thinning Blood Rheology on the Laminar-Turbulent Transition over a Backward Facing Step. **Fluids**, v. 5, n. 2, 2020. ISSN 2311-5521. DOI: 10.3390/fluids5020057.

KÉSMÁRKY, G. et al. Plasma viscosity: A forgotten variable. **Clinical hemorheology and microcirculation**, v. 39, p. 243–6, Feb. 2008. DOI: 10.3233/CH-2008-1088.

RAFIEIAN-KOPAEI, M. et al. Atherosclerosis: Process, Indicators, Risk Factors and New Hopes. **Int J Prev Med. 2014 Aug;5(8):927-46.**, 2014.

RAY, S.; ÜNSAL, B.; DURST, F. Development length of sinusoidally pulsating laminar pipe flows in moderate and high Reynolds number regimes. **International Journal of Heat and Fluid Flow**, v. 37, p. 167–176, 2012. ISSN 0142-727X. DOI: 10.1016/j.ijheatfluidflow.2012.06.001.

ROACHE, P. J. Quantification Of Uncertainty In Computational Fluid Dynamics. **Annual Review of Fluid Mechanics**, v. 29, n. 1, p. 123–160, 1997. DOI: 10.1146/annurev.fluid.29.1.123.

WAITE, L.; FINE, J. **Applied Biofluid Mechanics**. [S.l.]: The McGraw-Hill Companies, 2007. DOI: 10.1036/0071472177.

APPENDIX

A. INLET DATA GENERATOR SCRIPT

```
# ------------------------------------------------------------------------ #
#                        Inlet .csv file generator                         #
# ------------------------------------------------------------------------ #

# --------------------------------- 0 Imports ---------------------------- #

from math import sin, pi, ceil
from typing import Union

Number = Union[int, float]
# ------------------------------- 1 Functions ------------------------- #

def inletEquation(time: float, avgValue: Number, ampValue: Number, freq:
    Number, phaseLag: Number) -> Number:
    """Returns the flow velocity on the inlet, given a certain time

    Args:
        time (float): time value
        avgValue (Number): average value of senoidal wave
        ampValue (Number): amplitude value of senoidal wave
        freq (Number): frequency value
        phaseLag (Number): phase lag value

    Returns:
        Number: flow velocity on inlet
    """
    return avgValue + ampValue*sin(2*pi*freq*time + phaseLag)


# ---------------------------- 2 Inputs ------------------------------ #
#  2.1 File name
csvFileName: str = 'inlet.csv'

#  2.2 Velocity parameters
u_avg: Number = 7.7e-02      # Average inlet speed, in cm s
u_amp: Number = 7.7e-02      # Inlet speed magnitude, in cm s
theta: Number = 0            # Phase lag

#  2.3 Cardiac frequency
freq_bpm: int = 72              # in bpm
freq_Hz: Number = freq_bpm/60   # in Hz
period: Number = 1/freq_Hz      # Cardiac period, in s

#  2.4 Time parameters
deltaTime: Number = 1E-3                            # Time Step, in s
finalTime: Number = 20*period                         # Final Time, in s
NumberTimeSteps: int = int(finalTime/deltaTime)+1    # Number of time
    steps

# ----------------------- 3 Array Generation ----------------------- #
# 3.1 Time array
```

```
print('Creating time array...')
timeVector: list = [deltaTime * counter for counter in range(
    NumberTimeSteps)]

# 3.2 Velocity array
print('Creating velocity array...')
velocityVector = [inletEquation(
    t, u_avg, u_amp, freq_Hz, theta) for t in timeVector]


# -------------------------- 4 File creation ------------------------- #
print('Creating file...')
with open(csvFileName, 'w') as arquivo:
    for i in range(len(timeVector)):
        texto: str = str(timeVector[i]) + ',' + str(velocityVector[i]) +
    '\n'
        arquivo.write(texto)
```

B. $WSS_{x,cs}$ FOR EACH RHEOLOGICAL MODEL

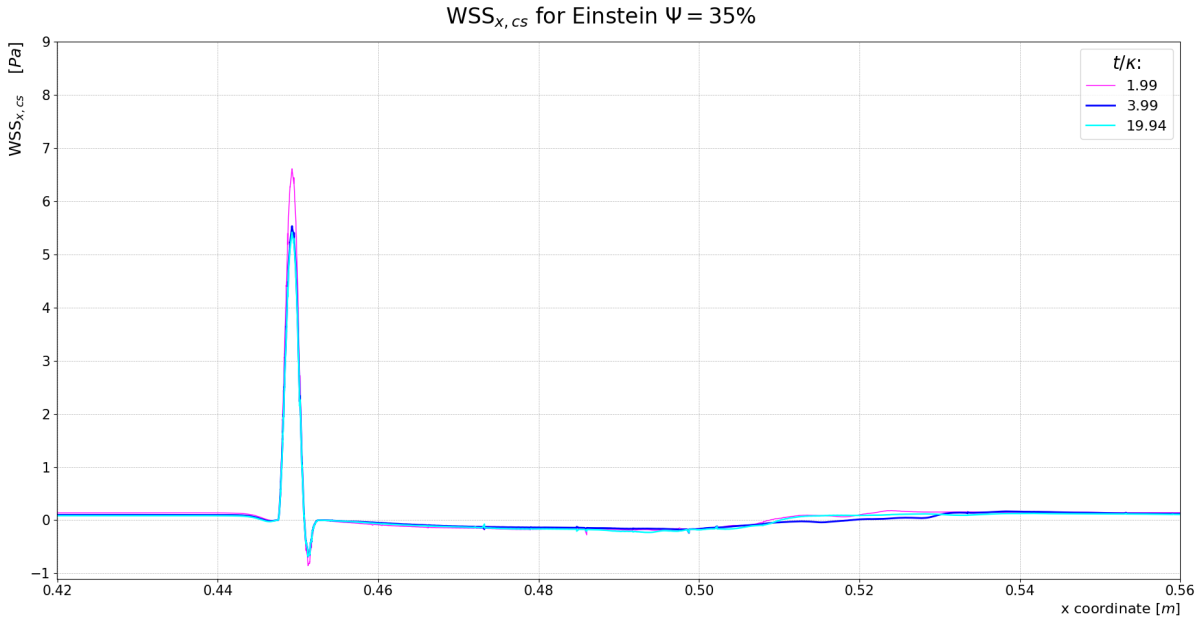

Figure 11 – $WSS_{x,cs}$ distribution for Einstein model considering $\psi = 35\%$

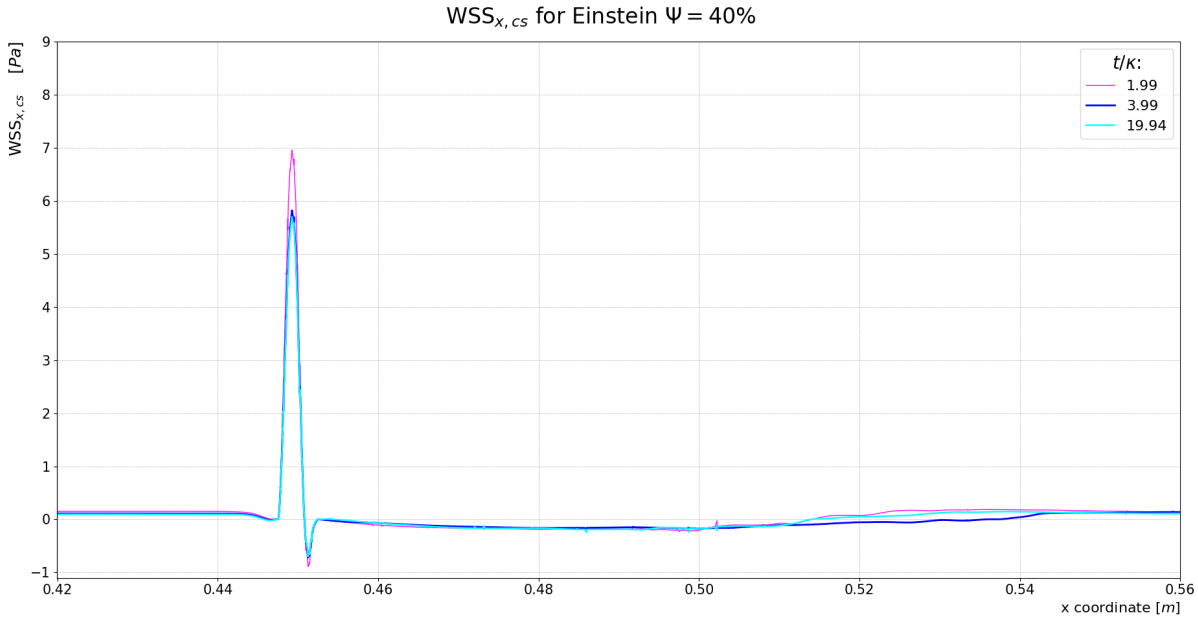

Figure 12 – $WSS_{x,cs}$ distribution for Einstein model considering $\psi = 40\%$

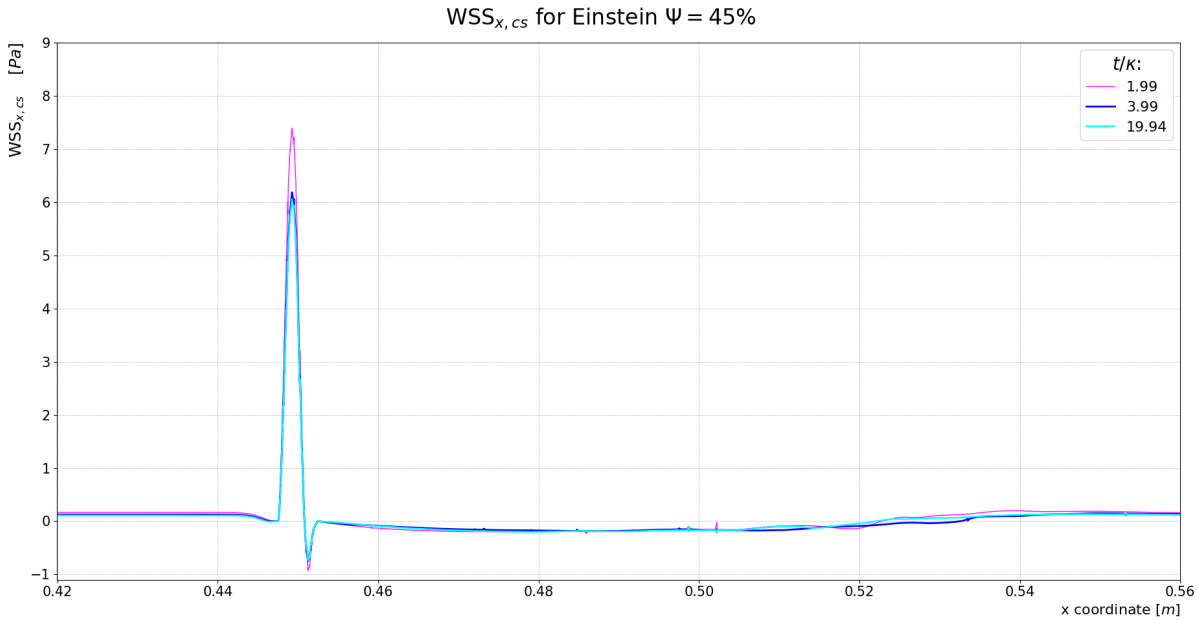

Figure 13 – $WSS_{x,cs}$ distribution for Einstein model considering $\psi = 45\%$

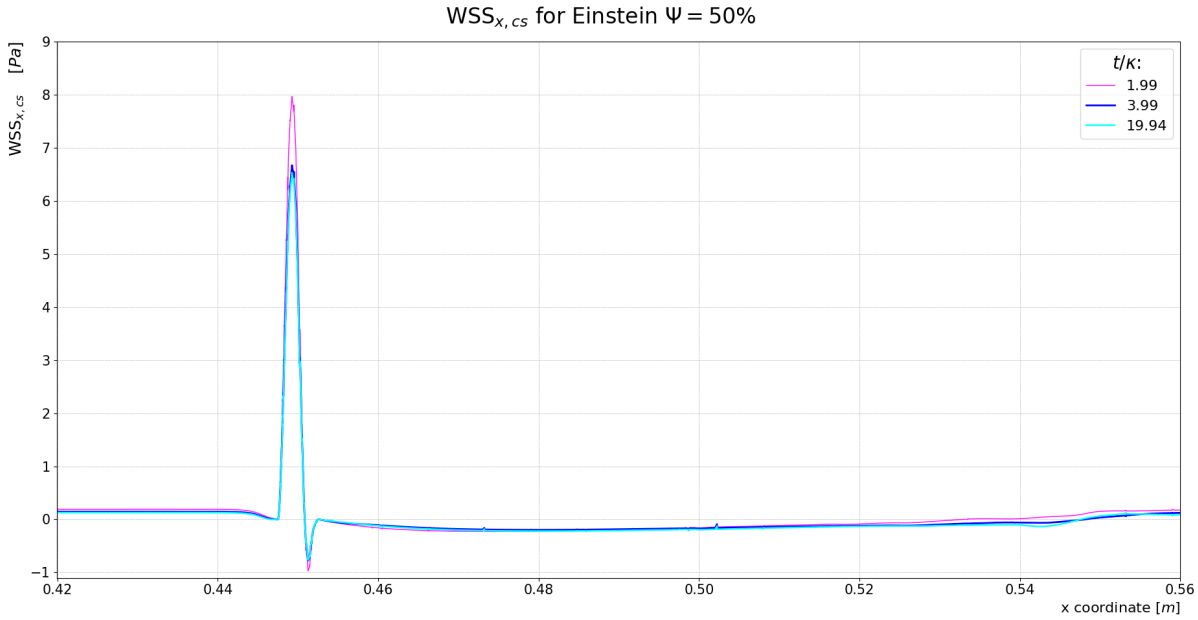

Figure 14 – $WSS_{x,cs}$ distribution for Einstein model considering $\psi = 50\%$

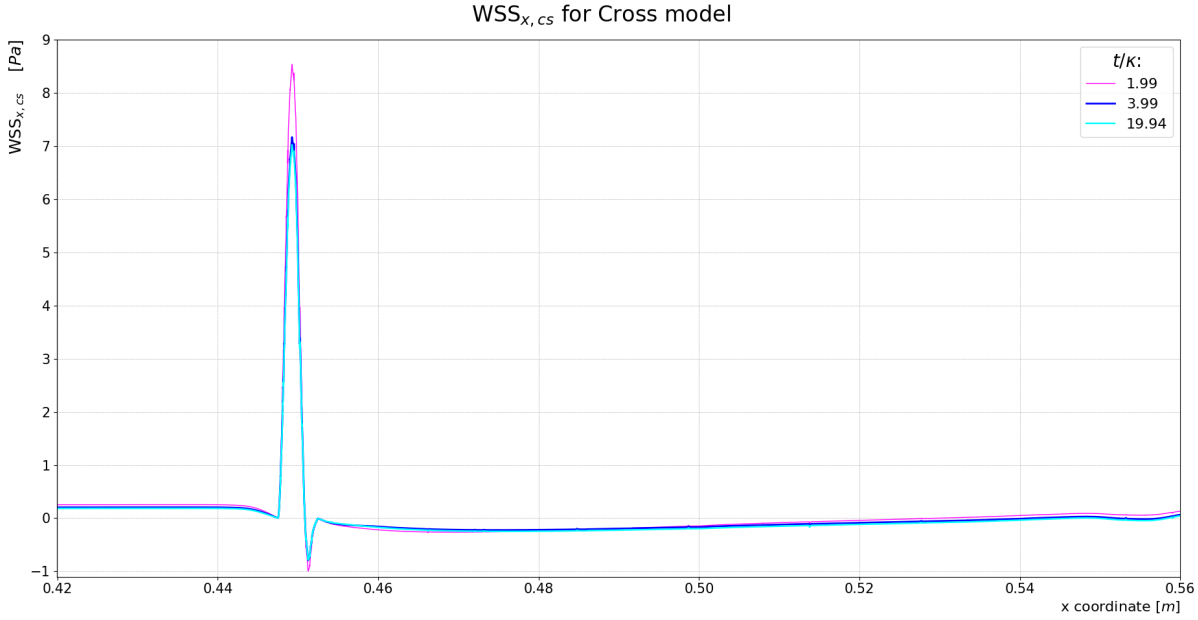

Figure 15 – $WSS_{x,cs}$ distribution for Cross model

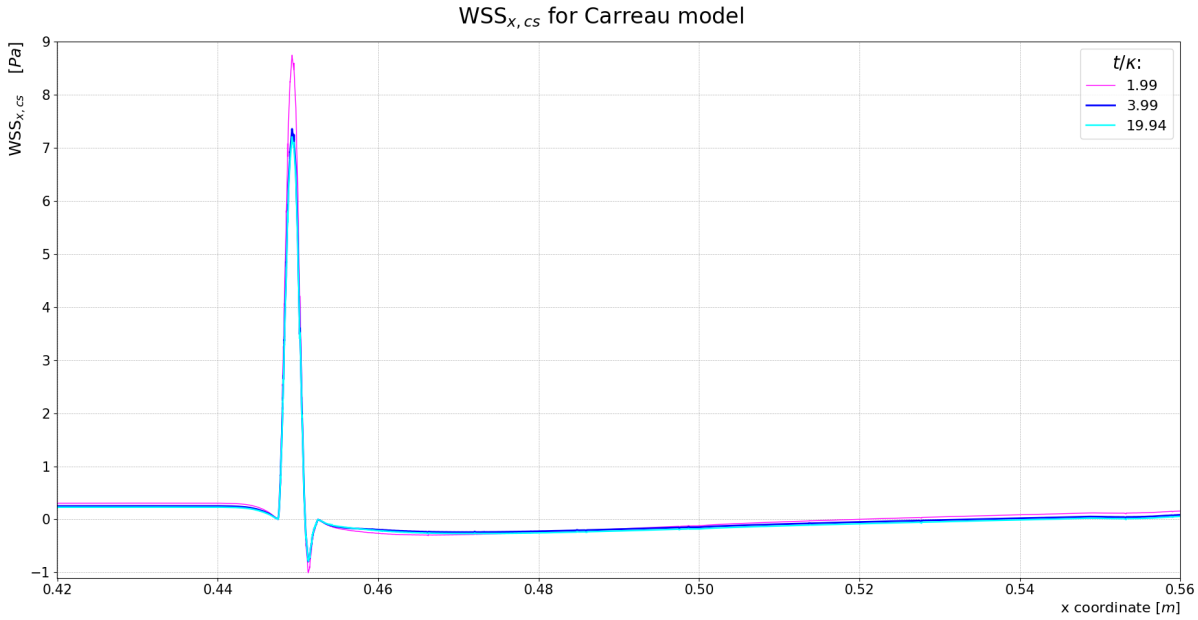

Figure 16 – $WSS_{x,cs}$ distribution for Carreau model